NeuroImage **16,** 1103–1119 (2002)
doi:10.1006/nimg.2002.1159

A Robust Transcortical Profile Scanner for Generating 2-D Traverses in Histological Sections of Richly Curved Cortical Courses

O. Schmitt[1] and M. Böhme

Institut für Anatomie, Medical University Lübeck, Ratzeburger Allee 160, D-23538 Lübeck, Germany

Received May 21, 2001

Quantitative analysis of the cerebral cortex has become more important since neuroimaging methods have revealed many subfunctions of cortical regions that were thought to be typical for only one specific function. Furthermore, it is often unknown if a certain area may be subdivided observer independently into subareas. These questions lead to an analytical problem. How can we analyze the cytoarchitecture of the human cerebral cortex in a quantitative manner in order to confirm classical transition regions between distinct areas and to detect new ones. Scanning the cerebral cortex is difficult because it presents a richly curved course and sectioning always leads to partially nonperpendicular sectioned regions of the tissue. Therefore, different methods were tested to determine which of them are most reliable with respect to generating perpendicular testlines in the cerebral cortex. We introduce a new technique based on electrical field theory. The results of this technique are compared with those of conventional techniques. It was found that straight traverses generated by the electrodynamic model present significantly smaller intertraversal differences than the conventional approaches.

Key Words: **cortex cerebri; mapping; profiles; traverses; transcortical scanning; image analysis; videomicroscopy; transparent flat bed scanning.**

INTRODUCTION

Quantifying the distribution of neurons of the human cortex cerebri has been carried out by image analysis (Adhami, 1973; Amunts *et al.*, 1995–2000; Geyer *et al.*, 1996–2000; Hudspeth *et al.*, 1976; Sauer, 1983; Schleicher *et al.*, 1978; Schleicher and Zilles, 1983; Semendeferi *et al.*, 1998; Wree *et al.*, 1981–1983) and morphometry followed by stereological estimation techniques (Haug, 1986; Holm and West, 1994; Pakkenberg and Gundersen, 1997; West, 1990, 1993; West and Gundersen, 1990; West and Slomianka, 1998; West *et al.*, 1988, 1991, 1993, 1994) since it provides architectural data derived from different techniques like histology, histochemistry, immunohistochemistry, and *in situ* hybridization. Image analysis is a powerful method that is useful for quantitative neuroanatomy because it enables the analysis of large and numerous cortical samples with high precision. Since the brain exhibits a complex three-dimensional structure, it would be desirable to perform structural analysis directly on a three-dimensional representation of the brain. However, methods such as the 3-D segmentation of overlapping projections of neuronal profiles within the histologic section space and classification of segmented neuronal profiles have high computational complexity and will cause most current systems to reach their limits. Three-dimensional approaches will be the methods of choice once sufficient computational power becomes available. For the moment, though, simple scanning procedures of the specimens like digitizing or scanning of profiles within the image can be considered as a method of low complexity that offers an adequate tool for quantitative analysis of neuronal tissue. If these data are obtained at a light microscopic or high scanner resolution level, cytoarchitectonic details become visible. Since cytoarchitecture can be considered as one of many modalities that characterize the individual architecture of different areas, it delivers the basic information for the detection of areal borders because the transition regions (Schleicher *et al.*, 1987, 1999, 2000; Schleicher and Zilles, 1990) between different areas can not be determined exactly by macroscopic features like the sulcus-gyrus pattern (Geyer *et al.*, 1996, 1999, 2000; Amunts *et al.*, 1999, 2000).

The distribution of neurons produces horizontal (lamination) and vertical (columnar) patterns within the cerebral cortex, which is a typical structural feature of the human brain. This inherent structure is used to subdivide the cerebral cortex into distinct areas. Cortical areas are delineated by the pial surface, cortex-white matter border and borders of neighboring areas. Neighboring cortical areas possess different cytoarchitectonic laminations. It is assumed that each

[1] To whom correspondence and reprint requests should be addressed. Fax: ++49 451 500 4034. E-mail: schmitt@anat.mu-luebeck.de.

1053-8119/02 $35.00

cortical area consists of a homogeneous distribution pattern of neurons or architecture. The characteristic homogeneous distribution pattern of neurons within a certain cortical area offers structural information which can be mapped in 3D-reconstructions (Amunts *et al.*, 2000; Geyer *et al.*, 1997, 1999, 2000; Roland and Zilles, 1998; Schmitt *et al.*, 1999a, 1999b; Schormann and Zilles, 1998; Zilles *et al.*, 1995). This kind of mapping is important for projections of functional features into the structural map and for locating and comparing different functions with different cytoarchitectonics.

Especially the lamination can be visualized and analyzed after digitizing and image processing of sections through the cerebral cortex. The quantitative analysis of the lamination is useful especially for observer independent delineation of cortical areas and the detection of their transition regions (Schleicher *et al.*, 1999, 2000). This kind of observer independent detection of areas appears to be valuable since there exists an extensive controversy over the location of cytoarchitectonically distinct cortical areas (Bailey and Bonin, 1951; Brodmann, 1909; Campbell, 1905; Economo and Koskinas, 1925; Sarkissov *et al.*, 1955; Smith, 1907). After digitizing histological sections (Schleicher and Zilles, 1990; Schmitt and Eggers, 1999), architectural data can be extracted by a geometric algorithm that operates on sets of very large images (Montgomery, 1996; Laroche, 1998). There exist several techniques to calculate orthogonal lines (traverses) to the pial surface of the cortex ending at the white matter border. Along these traverses the values of pixels of the image are read out and written into vectors which are also known as profiles. By analyzing such profiles we can extract structural information (distribution of local maxima and minima, points of inflection, shape) and use these parameters in order to characterize and quantitatively differentiate several types of horizontal distribution pattern, i.e., the lamination of different cortical areas (Amunts *et al.*, 1995–2000; Geyer *et al.*, 1996–2000; Schleicher *et al.*, 1987, 1999, 2000; Schleicher and Zilles, 1990; Semendeferi *et al.*, 1998; Wree *et al.*, 1981–1983). Consecutive profiles of a certain cortical area represent its quantified layering pattern and are called fingerprints; this term was introduced by Hudspeth *et al.* (1976). A traverse that lies exactly perpendicular to the lamination will lead to larger local gradients in the profile than traverses that have an oblique orientation to the principal direction of the lamination. The oblique traverse will produce a profile in which gradients are smaller, leading to some degree of blurring. If transition regions between areas are to be detected by a certain kind of analysis, for example a statistical test (Schleicher *et al.*, 1987, 1999, 2000; Schleicher and Zilles, 1990), then such blurring could influence the results. The influence is particularly strong if the lamination is presented by small gradients in the profile and/or by minor changes in the lamination pattern. Therefore, it is important to use an algorithm that calculates optimal traverses with respect to the principal orientation of laminae, even if they are arranged in a not completely parallel way.

Furthermore, the orientation of sections may vary according to the position of the tissue block in the embedding media. Even if we assume that the direction of sectioning is relatively orthogonal to the pial surface, its course is strongly curved. The profoundly convoluted cortical surface leads to the traverses-construction-problem (TCP): how should an orthogonal traverse be calculated? This problem is not trivial because tangentially sectioned regions are embedded in the richly curved convex-concave cortical surface (Griffin, 1994). Unsufficient orthogonality of traverses may influence the results of the averaged profiles and also statistical comparisons between them. Therefore, it is important to use a technique which generates robust orthogonal traverses. A further constraint is that traverses should not intersect, since intersections lead to distortions in the resulting profiles.

It is difficult, however, to give a precise mathematical definition of the traverses construction problem. The two constraints mentioned (orthogonality, no intersections) still allow a wealth of different solutions. For this reason, we will present parameters that can be used to measure traverse quality.

This study was motivated because intersections were frequently observed in traverses which were calculated using a centerline between the outer and the inner contour (Schleicher *et al.*, 1998, 1999; Schmitt *et al.*, 1998) of the curved regions of the cerebral cortex.

The objective of this study is to compare the results of different algorithms that generate traverses. A new technique has been developed that calculates traverses without considering special conditions or employing *a priori* knowledge about the curved cortical contour. Therefore, it works more reliably with respect to unforeseen geometrical situations and the resulting problems for those traverse calculation algorithms which minimize geometrical parameters (intersection angle of contours with the traverse, uniformity of traverse orientation, distance between traverses) (Schleicher *et al.*, 2000) or which employ smoothing steps and special algorithmic conditions to avoid traverse crossings at extremely curved parts of the inner and outer contours.

MATERIAL AND METHODS

A 65-year-old male human brain without any neuropathological changes was sectioned into 6112 coronal paraffin sections (human neuroscanning project). The postmortem delay was 11 h. The 20-μm-thick sections were stained in Gallocyanin chromalum (Schmitt and Eggers, 1997a). This staining has the advantage that perikarya of different regions in the sections are stained more homogeneously (Schmitt and Eggers, 1997b) than with the often used cresyl violet or silver staining method (Merker, 1983). However, further sections of a second specimen of a human brain (65-year-old female without any neuropathological changes; 12 h postmortem delay) around area 4 were produced and stained according to Merker (1983) in order to test the new algorithms under extreme conditions of cortical curvature. Inhomogeneous staining and section thickness variation either have to be avoided or corrected by applying the GLI-transformation (Schleicher and Zilles, 1990; Schleicher *et al.*, 2000) in order to obtain unbiased density profiles of the cortex. This was not performed here because the profiles were not analyzed for transition regions. The stained sections were digitized by a high resolution transparent flat bed scanner (FBS) (Agfa, Duoscan) as described by Schmitt and Eggers (1999). The resolution of the FBS images is 12.5 μm/pixel. The largest section has a size of about 11,000 $\times$ 7,000 pixels and a dynamic range of 8 bit. To test and develop the algorithms, an image of section 117 from the first brain was used; this is a section through the occipital lobe that includes areas 17 to 19. Later on, the algorithms were tested on more sections from both brains. For section 117, only one strongly curved section at the same cortical region was analyzed in all cases in order to obtain comparable results. The right hemisphere was cut out of the whole image (Fig. 1). This section exhibits good histological quality with respect to its thickness and size. Some smaller foldings within the white matter could not be avoided. However, these foldings do not substantially affect the resulting profile pattern. In the sample image the pial (outer border) and the white matter (inner border) contour were interactively marked using a MatLab script (MatLab 6) (Fig. 4). The result of this interactive step are two polygonal lines which are used later on to calculate the traverses. The points which are input by the user are connected by straight-line segments (linear interpolation); i.e., no spline interpolation or similar smoothing is performed.

Four different approaches to the traverses construction problem are considered in this study. The first involves stepping down a centerline between the inner and outer contours of the cortex and generating traverses which are orthogonal to the centerline and terminate at the contours (Schleicher *et al.*, 1999). The centerline was generated by connecting the midpoints of traverses generated using the electrodynamics algorithm described below. This technique should only be applied at relatively straight outer and inner contour paths. Therefore, it is of limited usefulness because gyrencephalic cortices possess strongly convex concave surfaces, and it will not be included in the statistical comparison of the various approaches. The second approach, which will be called the equal angles algorithm, generates traverses by minimizing the difference of the angles where the traverse intersects the inner and outer contour.

The third approach (Schleicher *et al.*, 2000) works by minimizing the length of the traverses and then employing corrective heuristics to optimize traverse placement.

The fourth approach uses a physical model based on electric field lines. Electric field theory and electrodynamic principles will not be described here since they have been published in great detail, e.g., in Feynman (1971), Zahn (1979), and Kraus (1984). The concept of electric field theory with respect to the problem of traverse calculation will be described briefly, and the formulae and algorithms to compute traverses will be presented in detail.

For the electrodynamics method, the inner and outer contour of the cortex are assumed to be electrically charged, one with a positive charge and the other with a negative charge. This leads to an electrical field around and in between the contours, the field lines originating on one contour and terminating on the other. These field lines will be used as traverses.

Electrical field lines exhibit several properties that make them suitable for determining traverses. First, it can be shown that field lines never intersect. This is obviously an important property and one which may be hard to attain using other approaches. However, note that intersections may occur if the field lines are not computed with sufficient accuracy. Second, the field lines intersect the contours at right angles. This property is also desirable, since the traverses should be perpendicular to the lamination pattern of the cerebral cortex. Third, field lines can be curved, reflecting the curvature of the inner and outer border of the cerebral cortex. However, straight lines can be generated easily if desired by connecting the points where the field lines intersect the contours.

As noted earlier, a contour C is a polygon; its vertices will be denoted by $\mathbf{c}^{(1)}, \ldots, \mathbf{c}^{(n)}$. To compute the electric field $\mathbf{E}_C$ of the entire contour, it is decomposed into straight-line segments, and the superposition of the fields for these individual segments yields the field for the entire contour. Thus, we have

$$\mathbf{E}_C(\mathbf{x}) = \sum_{j=1}^{n-1} \mathbf{E}_{\mathbf{c}^{(j)},\mathbf{c}^{(j+1)}}(\mathbf{x}),$$

where $\mathbf{x}$ is the point for which the field is to be computed. What remains is to determine $\mathbf{E}_{\mathbf{c}^{(j)},\mathbf{c}^{(j+1)}}$—the field of the charged line segment from $\mathbf{c}^{(j)}$ to $\mathbf{c}^{(j+1)}$. This can be obtained by integrating the field of a point charge

$$\mathbf{E}_{\mathrm{point}}(\mathbf{x}) = \frac{\mathbf{x}}{\|\mathbf{x}\|} \cdot \frac{1}{\|\mathbf{x}\|^2}$$

over the length of the line segment. (Constants have been omitted from the formula since they are not

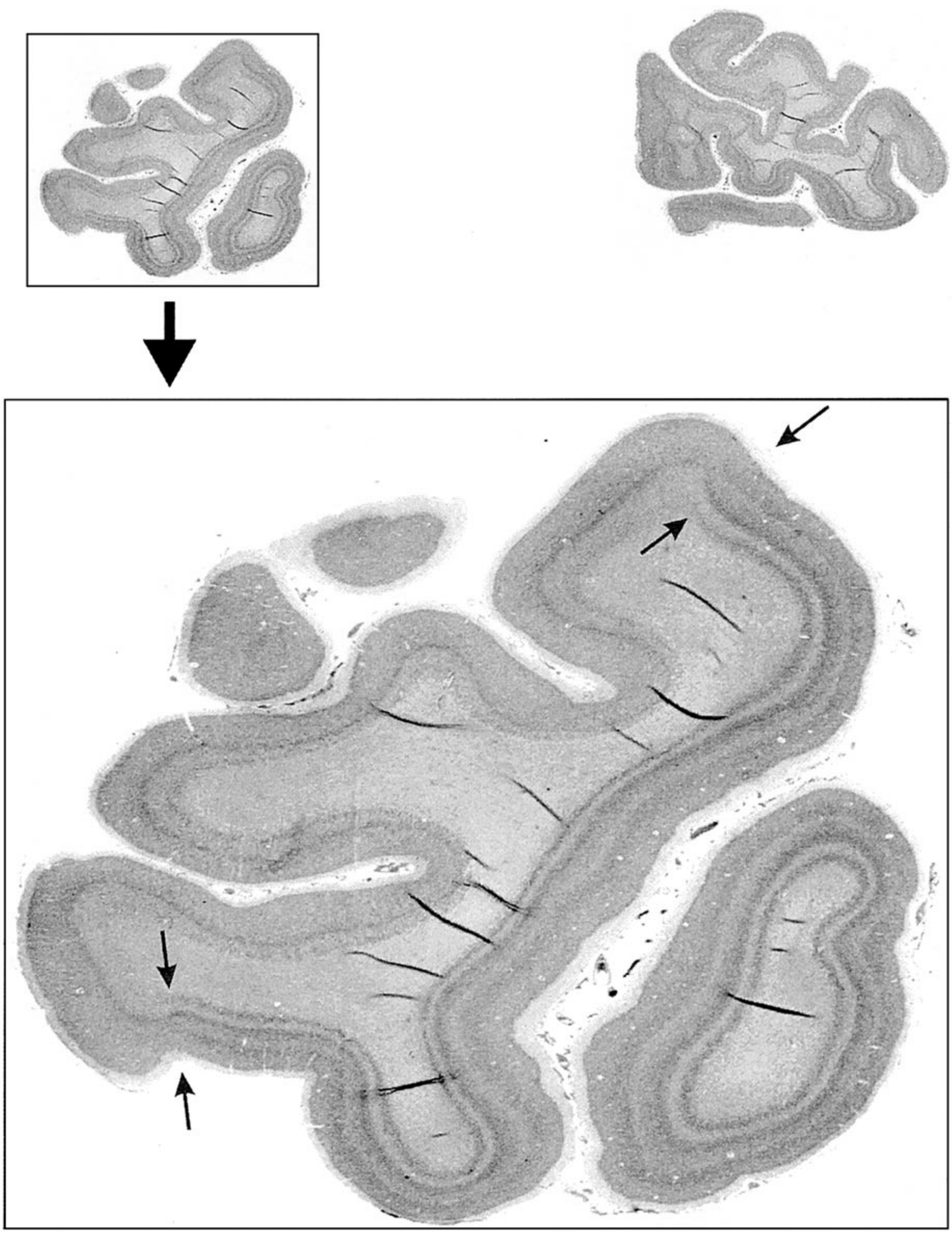

FIG. 1. Top: an FBS-image of a very large scale digital scan of section 117 through the human occipital lobe is shown. The images are mirrored because the analog object was projected during digitalization. Therefore, the left side of the section corresponds to the right side of the image. Below: an enlargement of the right occipital lobe. The transition regions of area 17 to 18 are marked by arrows. The enlarged sample image is used to test the algorithms.

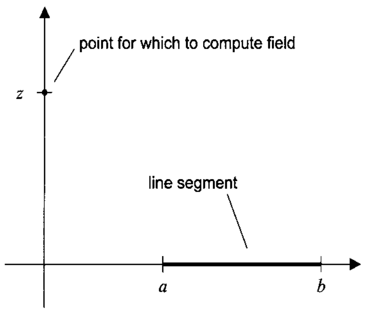

FIG. 2. Coordinate system chosen to facilitate computation of the electric field for a line segment. The line segment extends between coordinates a and b on the x-axis, the point for which the electric field is to be computed is at coordinate z on the y-axis.

needed in this context.) To facilitate the computation, a coordinate system is chosen that places the line segment on the x-axis and the point for which the electric field is to be computed on the y-axis (see Fig. 2). Integration of E_{point} then yields the horizontal and vertical components E_1 and E_2 of the electric field which are

$$E_1(a, b, z) = \frac{1}{\sqrt{z^2 + b^2}} - \frac{1}{\sqrt{z^2 + a^2}}$$

$$E_2(a, b, z) = \frac{1}{z}\left(\frac{b}{\sqrt{z^2 + b^2}} - \frac{a}{\sqrt{z^2 + a^2}}\right),$$

where the quantities a, b, and z are as indicated in Fig. 2.

In general, the line segments will be arbitrarily positioned within the coordinate system, and so a transformation of coordinate systems has to be made, the values for a, b, and z being obtained by projection of $\mathbf{c}^{(j)}$, $\mathbf{c}^{(j+1)}$, and $\mathbf{x}$ onto the vectors $\mathbf{p}$ and $\mathbf{n}$, which run parallel and normal to the line segment, respectively (see Fig. 3). The field of the line segment from $\mathbf{c}^{(j)}$ to $\mathbf{c}^{(j+1)}$ is thus

$$\mathbf{E}_{\mathbf{c}^{(j)},\mathbf{c}^{(j+1)}}(\mathbf{x}) = \begin{pmatrix} E_1(a, b, z) \cdot \mathbf{p} \\ E_2(a, b, z) \cdot \mathbf{n} \end{pmatrix}$$

where

$$\mathbf{p} = \frac{\mathbf{c}^{(j+1)} - \mathbf{c}^{(j)}}{\|\mathbf{c}^{(j+1)} - \mathbf{c}^{(j)}\|} = \begin{pmatrix} p_1 \\ p_2 \end{pmatrix}$$

$$\mathbf{n} = \begin{pmatrix} -p_2 \\ p_1 \end{pmatrix}$$

$$a = \langle \mathbf{c}^{(j)} - \mathbf{x}, \mathbf{p} \rangle$$

$$b = \langle \mathbf{c}^{(j+1)} - \mathbf{x}, \mathbf{p} \rangle$$

$$z = \langle \mathbf{x} - \mathbf{c}^{(j)}, \mathbf{n} \rangle,$$

where $\langle \cdot, \cdot \rangle$ denotes the scalar product. Finally, the respective fields for the two contours C_1 and C_2 are

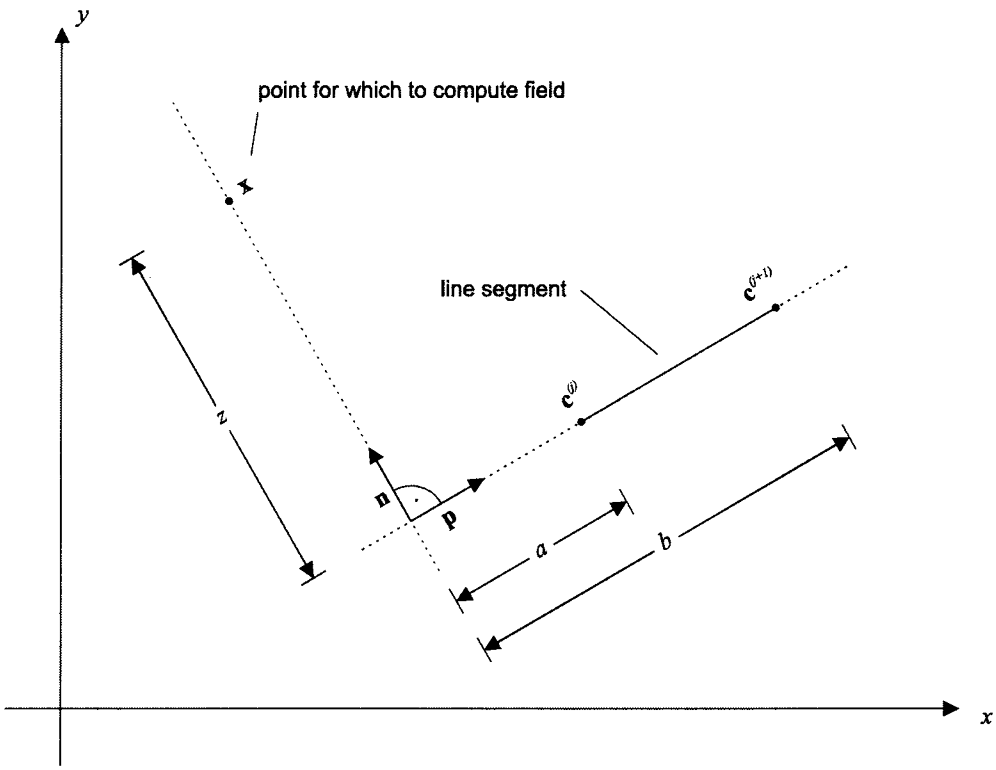

FIG. 3. Transformation of coordinate systems. Points $\mathbf{x}$, $\mathbf{c}^{(j)}$, and $\mathbf{c}^{(j+1)}$ are given with respect to the outer coordinate system (axes labeled x and y); the transformation yields their coordinates (z, a, and b, respectively) with respect to the coordinate system defined by vectors $\mathbf{p}$ and $\mathbf{n}$.

combined to give the total electric field $\mathbf{E}$; the field for the second contour is given a negative sign since the contours are oppositely charged. This yields

$$\mathbf{E}(\mathbf{x}) = \mathbf{E}_{C_1}(\mathbf{x}) - \mathbf{E}_{C_2}(\mathbf{x}).$$

This model will be referred to as the real physics model (RP).

A modification to this formula was derived that decreases the influence of a contour the closer the point $\mathbf{x}$ gets to it; this will be referred to as the modified electrodynamics model (MP). This model no longer reflects physical reality but has the advantage that the roughness of the contour has a weaker effect on the direction of the resulting traverse.

For this modified model, the above formula becomes

$$\mathbf{E}(\mathbf{x}) = \mathbf{E}_{C_1}(\mathbf{x}) \cdot \frac{d_{C_1}(\mathbf{x})}{d_{C_1}(\mathbf{x}) + d_{C_2}(\mathbf{x})} - \mathbf{E}_{C_2}(\mathbf{x}) \cdot \frac{d_{C_2}(\mathbf{x})}{d_{C_1}(\mathbf{x}) + d_{C_2}(\mathbf{x})}$$

where

$$d_C(\mathbf{x}) = (\min\{\|\mathbf{x} - \mathbf{c}^{(1)}\|, \ldots, \|\mathbf{x} - \mathbf{c}^{(n)}\|\})^{\alpha}$$

The quantity α is a parameter that can be used to control how strongly the influence of the closer contour is diminished. In the results presented here, a value of 0.8 was chosen for α.

A field line is computed by introducing a positive test charge close to the positively charged contour and then simulating the movement of the charge through the electric field. The traverse is now the path taken by the test charge or—optionally—a straight line between the points where this path intersects the contours. These two different methods of constructing traverses will be designated by the suffixes -C (for curved) and -S (for straight); this gives us four different variants of the electrodynamics algorithm: RP-S, RP-C, MP-S, and MP-C.

To compute the next field line, the starting point for the test charge is moved a fixed distance down the contour. This continues until the end of the contour is reached. The starting points are thus placed at equal distances along one of the contours.

In a region where the cortex is relatively straight, the distances between the traverses on the opposite contour will be approximately equal, too. However, in a region where the cortex is strongly curved, the traverses will be much closer together on the inside of the curve than on its outside. This leads to a problem if the starting points are on the inside contour. Within a strong curve, the distances between the traverses can become relatively large on the outside contour. For this reason, the algorithm described here will detect such a situation and react by exchanging the roles of the two contours. This means that the starting points for the test charges will move to the outside of the curve, ensuring that the traverses remain evenly spaced.

To simulate the movement of the test charge, iterative methods were used with the test charge moving in steps of a certain size. A sequence of points $\mathbf{t}_0$, $\mathbf{t}_1$, $\mathbf{t}_2, \ldots$ is thus computed, terminating when the test charge reaches the opposite contour.

For the iteration step, two different numerical methods were implemented (Schwarz, 1988). Initially, Euler's method was used, but the results were not sufficiently accurate. It was replaced with a second-order Runge–Kutta method, which delivered satisfactory results. For this method, the iteration step is

$$\hat{\mathbf{t}} = \mathbf{t}_i + \frac{\mathbf{E}(\mathbf{t}_i)}{\|\mathbf{E}(\mathbf{t}_i)\|} \cdot \frac{\delta}{2}$$

$$\mathbf{t}_{i+1} = \mathbf{t}_i + \frac{\mathbf{E}(\hat{\mathbf{t}})}{\|\mathbf{E}(\hat{\mathbf{t}})\|} \cdot \delta,$$

where δ is the size of the step to be taken.

It should be pointed out that the electrodynamic approach can easily be extended to three dimensions by replacing the charged contour lines with charged contour surfaces. The field lines can then be computed in exactly the same way as for the two-dimensional case.

RESULTS

Figure 1 shows the image through the right occipital lobe. The transition regions between areas 17 and 18 are marked by arrows. The inner and outer borders of the cortical region of interest are shown in Fig. 4. The figure also shows the traverses generated by the various algorithms. In comparing the four methods, the centerline algorithm (CL) appears to be the most error-prone. In regions of strong curvature, the traverses will often miss the inner contour and continue past it. This results in traverses which are much longer than their neighbors, are not orthogonal to the lamination and cross other traverses. These traverses are clearly unsuitable for the detection of transition regions.

In comparison, the equal angles algorithm (EA) produces better results (Fig. 4). However, intersections of traverses still occur; furthermore, in some cases there is a substantial difference in direction between neighboring traverses, even where the cortex is relatively straight and one would therefore expect to see roughly parallel traverses. This may likewise lead to difficulties in the detection of transition regions; quantitative data to support this will be presented further on.

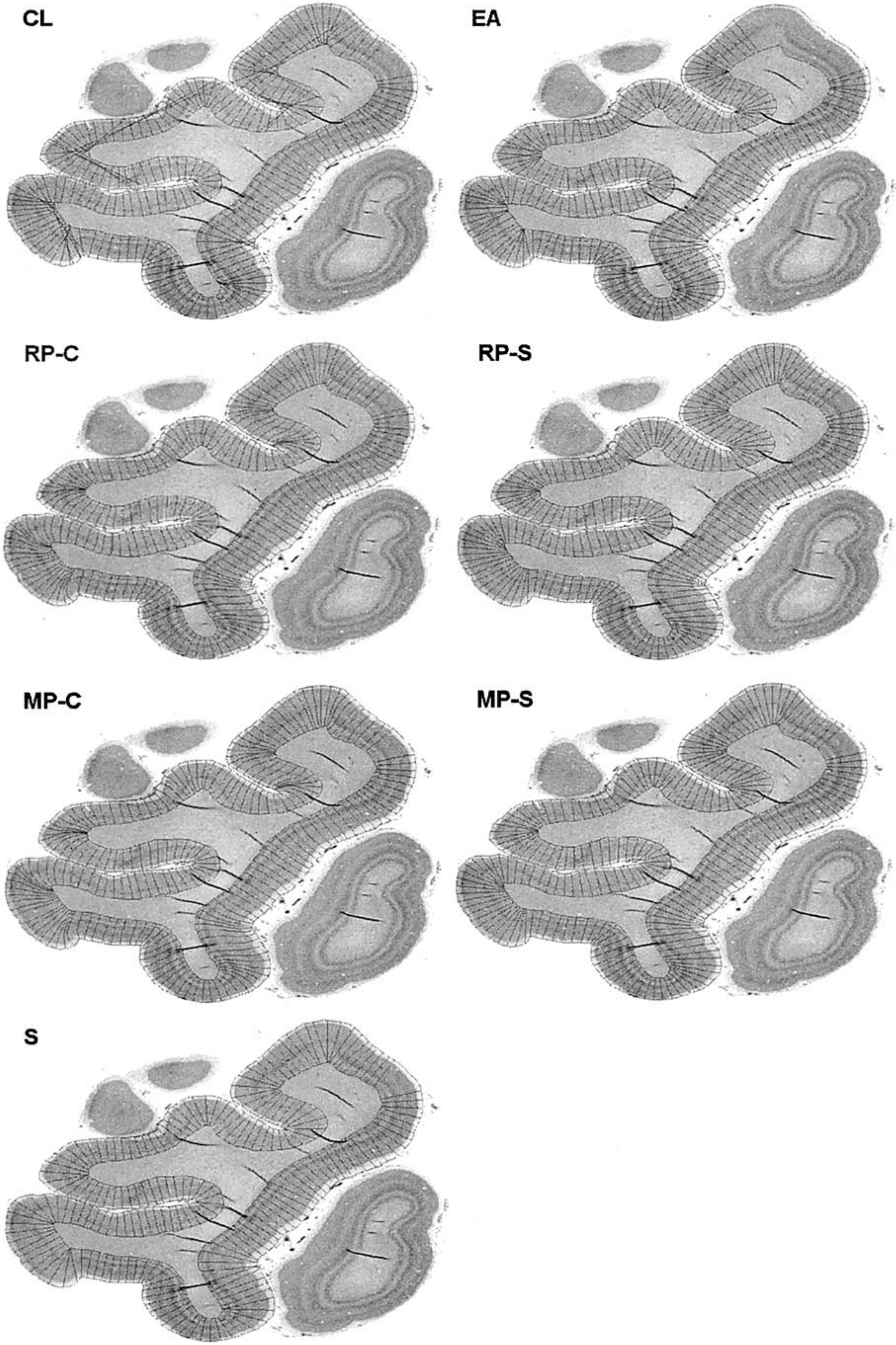

FIG. 4. All traverses are generated at a intertraverse distance of 40 pixels on the outer contour (pial surface). CL, centerline method. EA, equal angle method. RP, standard electrodynamic model (C, curved; S, straight). MP, modified electrodynamic model (C, curved; S, straight). S, length minimization technique of Schleicher *et al.* (2000). The centerline algorithm produces more degenerate traverses than the equal angles technique.

The undesirable properties of the equal angles and centerline algorithms are absent in the traverses generated by the electrodynamics algorithms (standard electrodynamics algorithm, straight (RP-S) and curved traverses (RP-C); modified electrodynamics algorithm, straight (MP-S) and curved (MP-C)) (Fig. 4). The results confirm the theoretical prediction that traverses generated in this way should not intersect.

The length minimization algorithm also produces traverses of good quality without intersections (Fig. 4).

To assess the quality of the traverses and thus of the fingerprint that was generated using them, we analyzed the differences between neighboring profiles.

The difference between two adjacent profiles can be expected to be quite small, especially since the columnar structure is not as clearly visible at the resolutions that were used as in videomicroscopic imaging. Furthermore, small columns have a thickness that corresponds to the diameter of pyramidal cells of the columns. When a traverse hits the border of a column then a large difference will result. Within the column, and this depends on the resolution of the image, the column diameter and the distance between the traverses, the differences of adjacent profiles will be of the same magnitude as outside the column. When the traverse hits the second border of a column, the second large difference will be measured. Because we compared different algorithms, all of them will pass the same structures and therefore comparable large profile intensity differences around columnar structures. At least, it is improbable that the majority of the columns are sectioned exactly parallel to the generated traverses, which would maximize profile intensity differences. Of course, there will always be a certain difference between the two traverses—otherwise, the fingerprint would be completely homogeneous in the horizontal direction.

If two different traverse sets have been produced for the same stretch of cortex, then it seems reasonable to consider those traverses as inferior that exhibit larger differences between neighboring profiles—on top of the differences which are inevitable because of the cortical structure, these traverses are generating excess differences, perhaps because they are not as well aligned as the traverses from the other set.

We therefore use profile differences as a measure of traverse quality—the smaller, the better. A second, derived parameter that we examine is the (numerically approximated) derivative of the profile differences. The motivation for this is the following: Along the fingerprint, the profile differences will vary in magnitude. Areas where the lamination pattern changes will produce larger profile differences, for instance. However, one would expect those profiles with large differences to be clustered together. An isolated large profile difference—corresponding to a large derivative—is indicative of a misplaced traverse.

In order to facilitate the comparison of the results of all traverse generators at different intertraverse distances (1, 2, 4, 8, 16, 32, 64 and 128 pixels), all fingerprints are summarized in Fig. 5. All profile lengths were normalized to 128 pixels. A plot directly below each fingerprint shows the profile differences across the width of the fingerprints. A second plot below the first shows the (approximated) derivative of the profile differences.

For small intertraverse distances, the electrodynamics algorithms produce differences that are much smaller than for the centerline and equal angles algorithms and slightly smaller than for Schleicher's length minimization algorithm. The derivative plots confirm these results.

The difference plots for large traverse distances are similar for all algorithms; this is because they are not very indicative of an algorithm's performance. Due to the distance between the traverses, there is no strong correlation between the relative alignment of two traverses and the magnitude of difference between the resulting profiles.

Three fingerprints and diagrams, those of the modified physics algorithm, centerline and equal angle method for traverse distance one, are shown in more detail in Fig. 6. Areal borders as well as the laminae can be assigned to the fingerprints. Typically those regions of the delineated cerebral cortex that have an intense curvature lead to strong disturbances in the fingerprint generated by the centerline algorithm as indicated by arrows in Fig. 6. Not optimally orientated traverses are produced by the equal angle technique, too. However, they do not occur as often as with the centerline method; some stronger disturbances in the fingerprint are indicated by arrows (Fig. 6).

In order to decide which algorithm produces the smallest differences between adjacent traverses, the maxima and mean values of the difference derivatives were computed (Table 1; Fig. 8). The length minimization algorithm is not able to generate meaningful traverses for large traverse distances, and so no results

FIG. 5. Cortical fingerprints of the gray level profiles of the traverses shown in Fig. 4. All methods are shown for intertraverse distances of 1, 2, 4, 8, 16, 32, 64, and 128 pixels. The two diagrams below each fingerprint plot the differences between adjacent profiles (top) and an approximation to the derivative of this difference graph (below). rp_s, standard electrodynamic model with straight traverses; rp_c, standard electrodynamic model with curved traverses; mp_s, modified electrodynamic model with straight traverses; mp_c, modified electrodynamic model with curved traverses; cl, centerline technique; ea, equal angles technique; s, length minimization technique of Schleicher *et al.* (2000). Algorithm *s* was not able to compute traverses at distance 128, therefore no results are given for this combination.

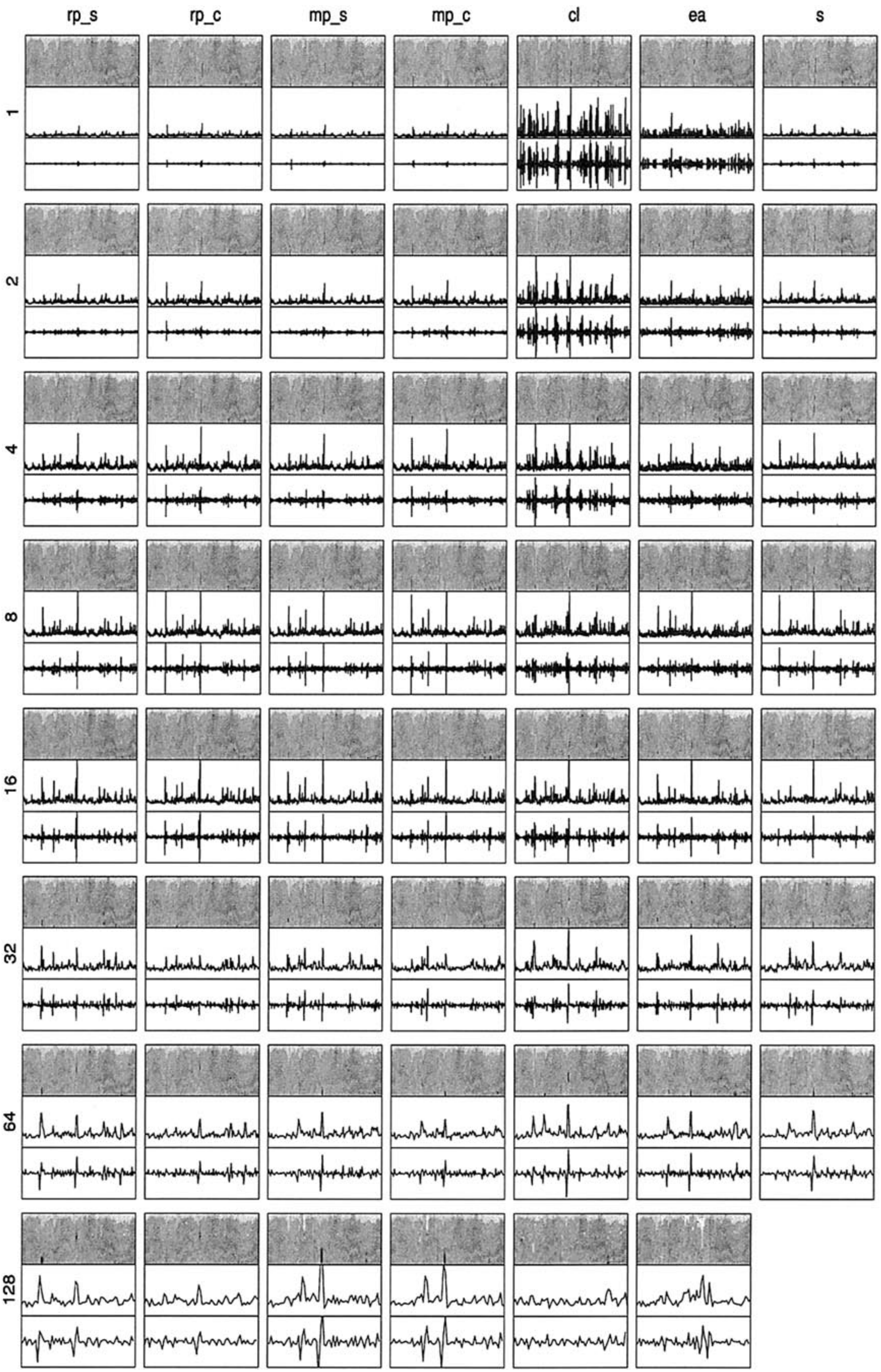
rp_s
rp_c
mp_s
mp_c
cl
ea
s
1
2
4
8
16
32
64
128

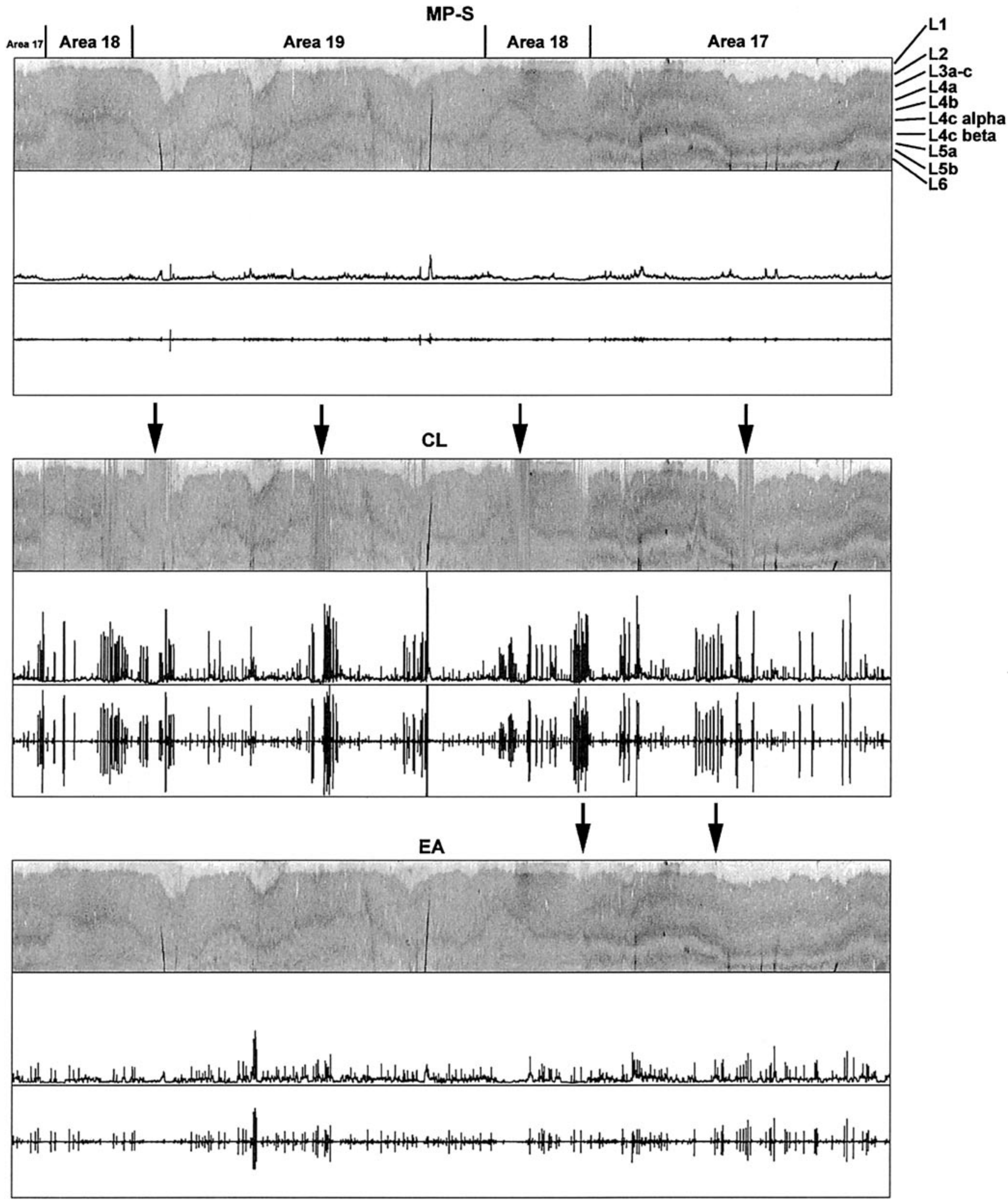

FIG. 6. A selection of cortical fingerprints from Fig. 5 with intertraverse distance one are shown here in greater detail. The MP-S method offers the best results followed by the RP-S method which is not shown here. The centerline (CL) and equal angle (EA) techniques show some disturbances in their fingerprints as indicated by arrows. The fingerprints of the three methods are scaled in the same way and can be compared directly. The top diagram below each fingerprint plots the differences between adjacent profiles which are largest for the CL method. The approximated derivative of the first plot is depicted in the second diagram. The differences are smaller for the equal angle technique and smallest for the MP-S method. The laminae are clearly visible and described in the MP-S fingerprint.

TABLE 1

Maximum and Mean Difference Derivatives of Gray Values of Adjacent Traverses

Distance	RP-S	RP-C	MP-S	MP-C	CL	EA	S
Maxima of derivative							
1	354	570	834	561	5715	2388	771
2	730	1691	950	1083	6675	2251	1547
4	1938	2537	1619	2450	5093	2329	2428
8	3175	5526	4241	4940	3863	2670	3260
16	4795	5239	4298	5017	3784	3114	3352
32	2594	1541	2484	2545	3315	2755	3042
64	2588	1831	2800	2004	3704	3114	2717
128	3179	1951	5333	4168	1529	2534	
Mean values of derivative							
Distance	RP-S	RP-C	RP-S	RP-C	CL	EA	S
1	26	27	27	28	142	51	43
2	71	75	73	76	194	106	99
4	141	144	139	147	247	179	164
8	199	204	197	211	286	230	225
16	260	263	262	262	336	265	268
32	298	258	287	263	346	306	308
64	362	327	328	294	390	354	345
128	477	406	673	570	450	475	

Note. Distance between two traverses is given in pixels. RP, original electrodynamic model; MP, modified electrodynamic model (S, straight traverses; C, curved traverses); CL, centerline; EA, equal angles; S, length minimization algorithm of Schleicher *et al.* (2000). Algorithm S was not able to compute traverses at distance 128, therefore no results are given for this combination. This table is visualized in Fig. 8.

are given for this algorithm at a traverse distance of 128. The centerline method yields the largest maxima and largest mean values, followed by the equal angle algorithm, the length minimization algorithm, and finally the electrodynamics algorithms. If distances between traverses are larger than four, the mean derivatives of the equal angle algorithm, the length minimization algorithm and the electrodynamic techniques lie close together. At an intertraverse distance of 64 pixels, the equal angle and length minimization algorithms produced slightly better results than the real physics model with straight traverses (RP-S).

Considering the mean derivatives from a realistic analytical point of view for intertraverse distances between 1 and 8 pixels, the straight traverses generated by the electrodynamic model are slightly better than the curved ones (Fig. 8). The standard (mean derivative: 26) and the modified (mean derivative: 27) electrodynamic models with straight traverses give the best results at an intertraverse distance of one pixel. The MP-S technique was also tested on sections from the second brain; two different cortical regions around area 4 that depict a strong curvature were analyzed (Fig. 7). These sections were stained according to Merker (1983). The fingerprints resulted from a one pixel intertraverse distance and the traverse illustrations from a 20 pixel distance. These examples do not show any crossings or misplaced traverses. The fingerprints show some major inhomogeneities resulting from the staining. This shows that a transformation of the image by the GLI method (Schleicher and Zilles, 1990) is necessary in order to obtain a homogeneous image.

Depending on the kind of transition regions that should be detected, an intertraverse distance between four and eight seems to give sufficient accuracy. If changes of the lamination patterns are located over a longer stretch of the cortex (area 4 to 6), an intertraverse distance of eight seems to be adequate, and if the transition region is small, like the one from area 17 to 18, an intertraverse distance of four can be selected.

Finally, the electrodynamic techniques, the equal angle procedure and the length minimization method of Schleicher *et al.* (2000) were tested on a segment of strongly folded cortex (Fig. 1). 17 consecutive sections were used in order to test the results of the techniques for statistically significant differences (*t* test). (The same stretch of cortex was used in all of the sections.) An intertraverse distance of one pixel was used for all techniques. Additionally, the length minimization algorithm was applied for an intertraverse distance of 0.75 in order to receive results comparable with the other techniques. This is necessary because this algorithm defines intertraverse distance as the distance between the traverse centers, whereas the other algorithms measure the distance on the outside contour. The results are summarized in Tables 2 and 3. The fingerprints and difference plots are presented in Fig. 9. The RP-S technique produces the smallest mean derivative of 40.4. Therefore, this technique was statistically compared with all other methods. RP-S produces significantly smaller difference derivatives in comparison to the equal angle and length minimization techniques (intertraverse distance 1.0). No significant difference was found between the length minimization algorithm using an intertraverse distance of 0.75 and the RP-S method. However, in every single section, RP-S produces smaller mean derivatives suggesting that an increase of the sample size would produce a significant difference.

DISCUSSION

Despite the fact that many analyses of the lamination of the cerebral cortex have been performed by scanning the lamination using traverses and calculating profiles (Adhami, 1973; Amunts *et al.*, 1995–2000; Geyer *et al.*, 1996–2000; Hudspeth *et al.*, 1976; Sauer, 1983; Schleicher and Zilles, 1983; Schleicher *et al.*, 1978–2000; Semendeferi *et al.*, 1998; Wree *et al.*, 1981–1983), there exists no precise algorithmical descrip-

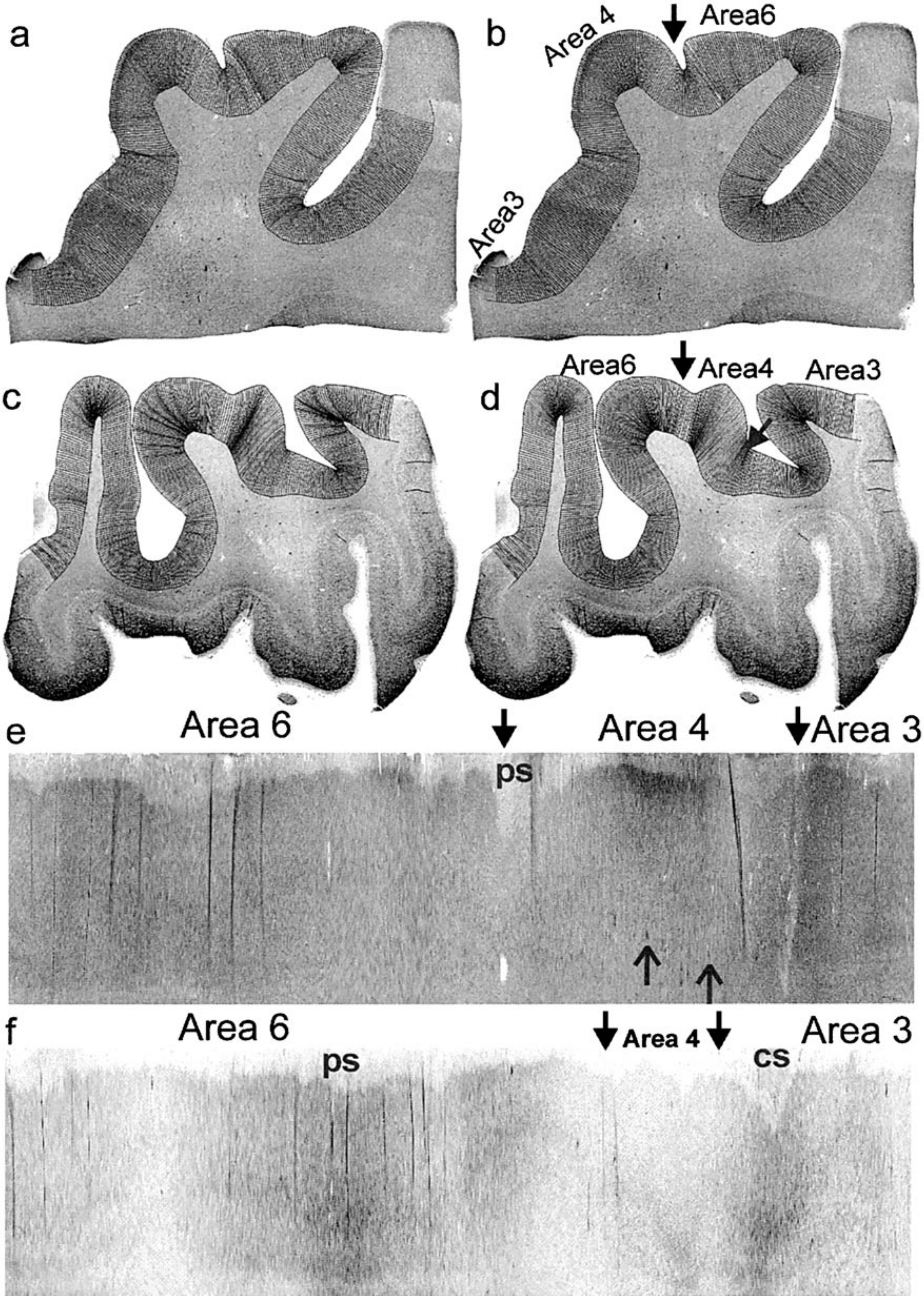

FIG. 7. Two further sections of the second human brain are used to test the algorithms in order to show the reliability of traverse generation in richly curved parts of the cerebral cortex. The sections, which are 20 μm thick and stained according to Merker (1983), were produced from blocks located around the central sulcus. (a) and (b) are taken from a block which was sectioned at the convexity of the brain. (a) Shows the result of the MP-C technique and (b) that of the MP-S method. (c) and (d) are from a block taken just above area 43. Therefore, the insular region has been partially cut off at the bottom of the images. The MP-S method was applied to the image of the convexity section at an intertraverse distance of one pixel. (c) Shows the result of the MP-C technique and (d) that of the MP-S method. The fingerprints for the two sections (generated using MP-S) are shown in (e) and (f). The inhomogeneous staining of the Merker methods is also visible in the fingerprints. ps, precentral sulcus; cs, central sulcus.

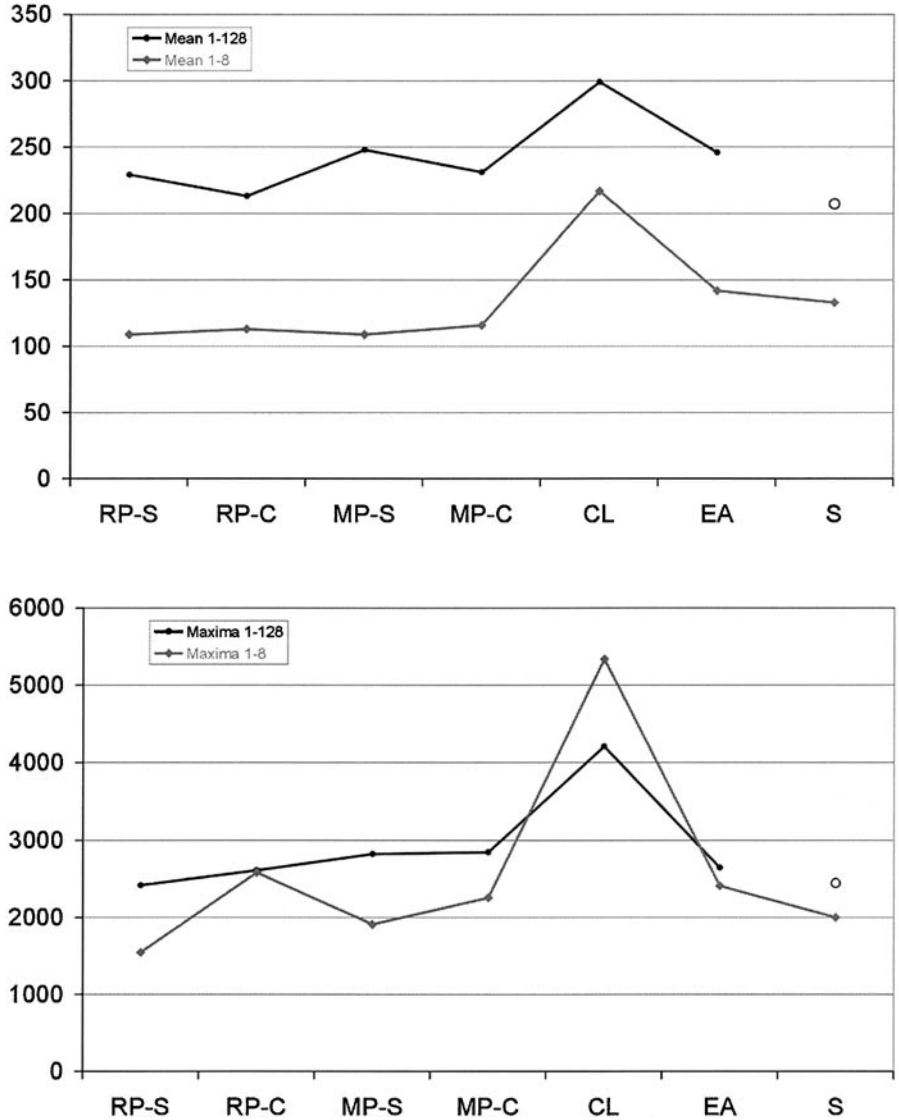

FIG. 8. The two diagrams plot the traverse difference derivatives from Table 1 averaged over two groups of intertraverse distances: the first group (1–128) contains all the intertraverse distances, the second (1–8) contains intertraverse distances 1 to 8. (The *S* algorithm aborted with intertraverse distance 128, so it was not included in the 1–128 group. This favors the *S* algorithm in this group, since the other algorithms are penalized by large values for intertraverse distance 128. To indicate this, the data points for the *S* algorithm are drawn as hollow circles.) The top diagram shows averaged mean derivatives, the bottom diagram shows averaged maximum derivatives. In this diagram, the curves cross at CL because its differences become lower with an increase of the intertraverse distances. The intertraverse distances of the second group can be recomended for profile generation because they present the smallest differences, and the values of the electrodynamics methods lie close together. According to Table 1, applying the MP-S technique with an intertraverse distance of 4 pixels seems to be a compromise with respect to intertraverse grey value differences and computational requirements.

tion. Because the traverse scanning technique is used as a first step for delineating the complex pattern of cortical areas and further analyses like determination of areal variability, sex differences, intra- and interindividual variations (Amunts *et al.*, 1995–2000; Geyer *et al.*, 1996–2000; Schleicher *et al.*, 1987, 1999, 2000; Schleicher and Zilles, 1990; Semendeferi *et al.*, 1998; Wree *et al.*, 1981–1983), it is important to use transparent computational techniques. Distortions of profiles resulting from traverse generation by the centerline or equal angle algorithms may influence further statistical analysis and automatic detection of transition regions between different cortical fields. Furthermore, the laminar pattern is distorted (Fig. 6) and does not run perfectly parallel to the cortical surface. This can be explained, at least in part, by the effect of cortical folding on the laminar pattern. An additional source of variability, however, is introduced by the variation in depth of lamina 1. The reconstruction of a part of the laminar pattern and, hence, the calculation

TABLE 2

Maximum Derivatives of Sections 116 to 132

S-no.	RP-S	RP-C	MP-S	MP-C	EA	S1	S075
116	1464	1610	1326	1530	3679	425	254
117	1435	1304	678	600	4482	425	280
118	1098	1211	1374	1605	3092	441	342
119	1883	2089	357	328	3127	548	430
120	926	678	440	1255	3119	525	394
121	281	263	1866	1565	3509	380	304
122	2219	1802	416	416	5101	1163	1304
123	599	769	2164	2337	3673	1043	1150
124	1727	1800	915	1395	3920	1460	685
125	2875	4034	3737	4046	4840	1027	4936
126	1771	1675	953	799	5064	1933	770
127	1539	1871	2173	2352	4253	18370	381
128	1863	2403	2623	3242	4211	1036	1413
129	240	542	1086	1177	1589	24910	128
130	2601	2781	2379	2924	5819	615	448
131	2757	2956	2784	3012	4417	1967	5083
132	2345	2570	2390	2348	6537	935	678
MV	1624.9	1785.8	1627.1	1819.5	4143.1	3364.9	1116.5
STD	807.6	976	980.2	1069	1161.8	6992.5	1512.6

Note. S1, the algorithm of Schleicher *et al.* (2000) with an intertraverse distance at the centerline of one pixel. S075, the same algorithm as used by S1 but with an intertraverse distance at the centerline of 0.75 pixels. S-no., number of the histologic section. MV, mean value. STD, standard deviation.

of traverses, would be improved by defining the outer border at the lamina 1/lamina 2 transition. However, information will be lost since lamina 1 could be important because changes of the density of nerve fibers are an indirect indication for structural differences between adjacent areas, even though axon collaterals do not show up in the stainings used here.

Algorithms that generate traverses have previously been described in the literature. Schleicher *et al.* (1998, 1999) give a description of a centerline based algorithm, but the description there is quite vague, basically mentioning only the fact that a centerline is used. One may suspect that this approach uses additional heuristics to detect cases where misplaced traverses have been generated, since the centerline algorithm is prone to such errors, as demonstrated here. However, no mention of any corrective heuristics is made by the authors. Special corrections to optimize misplaced traverses generated by the centerline algorithm are possible. For example, if traverses do cross they can be rotated until they do not cross anymore. Furthermore, the inner and outer border can be shortened after a new traverse has been generated so that new traverses are calculated for the rest of the border. This reduction can be applied to a kind of frame of the inner and outer border, too (Schmitt *et al.*, 1998). The CL and EA techniques tested here are not implemented to use corrections because they are not described in Schleicher *et al.* (1998, 1999) in a comprehensible way.

A more recent publication (Schleicher *et al.*, 2000) describes a different algorithm based on minimizing traverse length combined with additional heuristics designed to optimize traverse placement. As demonstrated, this algorithm produces traverses of good quality. However, the description of the algorithm as published is quite sketchy; implementing the algorithm required a significant amount of experimentation to discover details that were not immediately obvious but turned out to be vital to make the algorithm work correctly. Also, the fact that the algorithm needs heuristics to ensure adequate traverse placement may mean that unsatisfactory results could be generated in situations for which the algorithm has not been tested and for which no corrective procedures have been developed. In fact, while processing the series of 17 sections, we discovered that the algorithm would abort if it ran into a strong bend in the contour that had been input using only a few contour points. To make the algorithm run correctly, the bend had to be smoothed by inserting more contour points. The other algorithms did not exhibit this problem.

The electrodynamics algorithm produces satisfactory results even for difficult cortex geometries (Griffin, 1994) without requiring the use of corrective heuristics. It can therefore be expected to perform robustly even in situations for which it has not been tested. Quantitative data have been presented that demon-

TABLE 3

Mean Derivatives of Sections 116 to 132

S-no.	RP-S	RP-C	MP-S	MP-C	EA	S1	S075
116	34	34	37	35	65	76	51
117	38	39	40	39	70	63	42
118	23	24	26	25	49	43	28
119	35	36	38	35	70	61	40
120	43	45	46	44	77	75	49
121	32	32	35	33	61	56	36
122	36	37	38	36	73	63	41
123	46	46	51	48	78	79	52
124	49	50	52	49	87	90	59
125	74	76	80	75	117	126	84
126	43	43	45	44	73	75	49
127	35	36	37	36	57	10	39
128	54	57	57	56	90	93	60
129	18	19	19	19	34	10	25
130	45	46	47	46	81	78	49
131	35	36	36	35	67	60	39
132	47	48	49	47	68	80	51
MV	40.4	41.4	43.1	41.3	71.6	66.9	46.7
STD	12.6	12.9	13.4	12.6	17.9	28.1	13.6
Sign.		0.82	0.55	0.84	1.5×10^{-6}	0.001	0.17

Note. The confidence level (t test) is shown in the last row. The results of all algorithms were compared with the RP-S result. The EA and the S1 results are significantly different (significance level 0.05) in comparison to the RP-S technique. S-no., number of the histologic section. MV, mean value. STD, standard deviation.

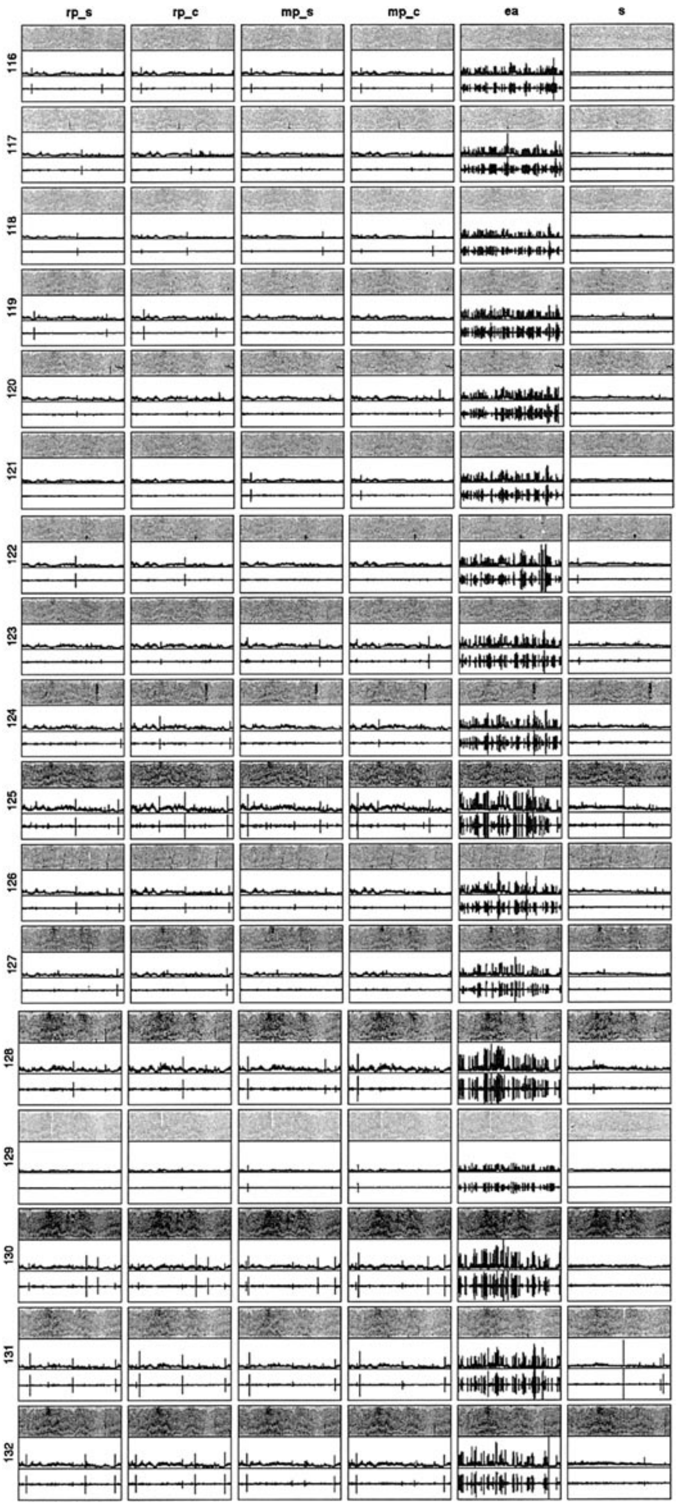

FIG. 9. The same cortex segment in histologic sections 116 to 132 was used for generating traverses. The intertraverse distance of the electrodynamic methods (rp_s, rp_c, mp_s, mp_c) and of the equal angle method was 1.0 pixel. The length minimization algorithm (s) used an intertraverse distance of 0.75 pixels. The accompanying difference derivatives are listed in Tables 2 and 3.

strate the superiority of this approach over the other approaches that were studied where the continuity of the generated gray level profiles is concerned.

The electrodynamics algorithm has no influence on the effect of extremely tangentially sectioned cups of gyri or sulci. If the generator passes such an extreme region, certain laminae are represented too strongly or too weakly compared to a perpendicularly sectioned part of the same region. Maybe this problem of non-linear distortions resulting from non-orthogonal sectioning of the cerebral cortex can be corrected by a non-linear normalization of the profiles. A prerequisite for such a tangential correction would be a reliable detection of laminar borders within a profile followed by the identification of discontinuities or even jumps in the laminar heights between neighboring profiles.

The electrodynamic approach that was tested on 2-D surface data here can easily be adapted to 3-D volume data. This seems to be an obvious advantage in comparison to the techniques based on geometric algorithms. If we are able to register such high-resolution images of serial histologic sections of up to 10^9 pixels, which is close to the resolution of single cells, then we can easily adapt and apply the electrodynamic algorithm for orthogonal scanning of the cerebral cortex in the resulting 3-D volume data. Naturally, under such circumstances the tangential section problem would not occur any more.

In Figs. 4, 7a, and 7b two different parts of the cerebral cortex were analyzed. The fact that Fig. 4 shows a gallocyanin chromalum stained section and Figs. 7a–7d a Merker stained one of different individuals is not relevant here, since we aimed to document only that the MP-S and MP-C methods work properly on richly curved cortical contours. Because it has already been shown in the example of a more smooth cortical surface in Fig. 4 that the CL and EA algorithms produce strong intersections of traverses we forego testing the results on a much more curved part of the cortical surface (Figs. 7c–7d).

A further idea for quantifying the lamination pattern of the cerebral cortex is the tesselation of the area in between the outer and inner border. Orthogonal stacks of tesselated polygons may present an alternative method for quantifying the cortical lamination (Duyckaerts *et al.*, 1994; Grignon *et al.*, 1998). Bok (1959) has already described a tesselation of the area between the outer and inner border of the cerebral cortex by a regular chessboard pattern.

Another possibility for lamination analysis could be the application of elasticity theory (Budó, 1990; Landau and Lifshitz, 1959; Sokolnikoff, 1956). Convexities and concavities can be considered as force vectors that have to be minimized in order to unfold the 2-D projection of the cortical area.

Different authors (Carman *et al.*, 1995; Fischl *et al.*, 1999; Xu *et al.*, 1999) have already applied surface modeling methods (outline-based (Levinthal and Ware, 1972; Christian and Sederberg, 1978) and/or volumetric-based (Lorenson and Cline, 1987)) followed by the analysis of flat maps (Griffen, 1994; Haidekker *et al.*, 1998; Jouandet *et al.*, 1989; Schwartz and Merker, 1986; Van Essen and Maunsell, 1980) of the surface of the human brain. It would be a great advantage to use these nonlinear transformation techniques to produce flat cytoarchitectonic maps of the human cerebral cortex, which would offer new perspectives in statistical evaluation and comparative inter- and intraindividual studies.

In this study, columnar patterning (Mountcastle, 1997), for example that of the primary motor cortex, is not considered. A possibility for quantifying the columnar patterning could be the construction of testlines between traverses (parallel to the inner and outer border) generated by the modified electrodynamic model with straight traverses.

After calculating the profiles they can be normalized to a certain length. So far this is done by linear interpolation. We can suppose that local morphologic features like convexity and concavity measures may be used in order to obtain a better normalization of the cortical region of interest. This would be very helpful at those regions of a section that have been cut in a more or less tangential manner.

In summary, the electrodynamics algorithms generate robust profile families even within extreme courses of the inner and outer surface of the cerebral cortex.

REFERENCES

Adhami, H. 1973. Die photometrische Bestimmung des Cortexzell- und Graugehalts auf der Grundlage des Nissl-Bildes. *Acta Anat.* **84:** 1–52.

Amunts, K., Istomin, V., Schleicher, A., and Zilles, K. 1995. Postnatal development of the human primary motor cortex: A quantitative cytoarchitectonic analysis. *Anat. Embryol.* **192:** 557–571.

Amunts, K., Schmidt-Passos, F., Schleicher, A., and Zilles, K. 1997. Postnatal development of interhemispheric asymmetry in the cytoarchitecture of human area 4. *Anat. Embryol.* **196:** 393–402.

Amunts, K., Schleicher, A., Bürgel, U., Mohlberg, H., Uylings, H. B. M., and Zilles, K. 1999. Broca's region revisited: Cytoarchitecture and intersubject variability. *J. Comp. Neurol.* **412:** 319–341.

Amunts, K., Malikovic, A., Mohlberg, H., Schormann, T., and Zilles, K. 2000. Brodmann's areas 17 and 18 brought into stereotaxic space—Where and how variable? *NeuroImage* **11:** 66–84.

Bailey, P., and von Bonin, G. 1951. *The Isocortex of Man.* University of Illinois Press, Urbana.

Bok, S. T. 1959. *Histonomy of the Cerebral Cortex.* Elsevier, Amsterdam.

Brodmann, K. 1909. *Vergleichende Lokalisationslehre der Grosshirnrinde in ihren Prinzipien dargestellt auf Grund des Zellenbaues.* Barth, Leipzig.

Budo, A. 1990. *Theoretische Mechanik.* VEB Deutscher Verlag der Wissenschaften, Berlin.

Campbell, A. W. 1905. *Histological Studies on the Localization of Cerebral Function.* Cambridge Univ. Press, Cambridge.

Carman, G. J., Drury, H., and Van Essen, D. 1995. Computational methods for reconstructing and unfolding the cerebral cortex. *Cereb. Cort.* **5:** 506–517.

Christian, H. N., and Sederberg, T. W. 1978. Conversion of complex contour line definitions into polygonal element mosaics. *Comp. Graph.* **12:** 187–192.

Duyckaerts, C., Godefroy, G., and Haiw, J.-J. 1994. Evaluation of neuronal numerical density by Dirichlet tesselation. *J. Neurosci. Methods* **51:** 47–69.

Feynman, R. P. 1971. *Lectures on Physics*, Vol. 2. Addison-Wesley, Reading.

Fischl, B., Sereno, M. I., and Dale, A. M. 1999. Cortical surface-based analysis II: Inflation, flattening, and a surface-based coordinate system. *NeuroImage* **9:** 195–207.

Geyer, S., Ledberg, A., Schleicher, A., Kinomura, S., Schormann, T., Bürgel, U., Klingberg, T., Larsson, J., Zilles, K., and Roland, P. E. 1996. Two different areas within the primary motor cortex of man. *Nature* **382:** 805–807.

Geyer, S., Schleicher, A., and Zilles, K. 1997. The somatosensory cortex of human: Cytoarchitecture and regional distributions of receptor-binding sites. *NeuroImage* **6:** 27–45.

Geyer, S., Matelli, M., Luppino, G., Schleicher, A., Jansen, Y., Palomero-Gallagher, N., and Zilles, K. 1998. Receptor autoradiographic mapping of the mesial motor and premotor cortex of the macaque monkey. *J. Comp. Neurol.* **397:** 231–250.

Geyer, S., Schleicher, A., and Zilles, K. 1999. Areas 3a, 3b, and 1 of human primary somatosensory cortex. 1. Microstructural organization and interindividual variability. *NeuroImage* **10:** 63–83.

Geyer, S., Schormann, T., Mohlberg, H., and Zilles, K. 2000. Areas 3a, 3b and 1 of human somatosensory cortex: 2. Spatial normalization to standard anatomical space. *NeuroImage* **11:** 684–696.

Griffin, L. D. 1994. The intrinsic geometry of the cerebral cortex. *J. Theor. Biol.* **166:** 261–273.

Grignon, Y., Duyckaerts, C., Bennecib, M., and Hauw, J. J. 1998. Cytoarchitectonic alterations in the supramarginal gyrus of late onset Alzheimer's disease. *Acta Neuropathol. Berl.* **95:** 395–406.

Haug, H. 1986. History of neuromorphometry. *J. Neurosci. Methods* **18:** 1–17.

Haidekker, M. A., Evertsz, C. J. G., Fitzek, C., Boor, S., Andresen, R., Falkai, P., Stoeter, P., and Peitgen, H.-P. 1998. Projecting the sulcal pattern of human brains onto a 2D plane—A new approach using potential theory and MRI. *Psych. Res. Neuroimag.* **83:** 75–84.

Holm, I. E., and West, M. J. 1994. Hippocampus of the domestic pig: A stereological study of subdivisional volumes and neuron numbers. *Hippocampus* **4:** 115–125.

Hudspeth, A. J., Ruark, J. E., and Kelly, J. P. 1976. Cytoarchitectonic mapping by microdensitometry. *Proc. Natl. Acad. Sci. USA* **73:** 2928–2931.

Jouandet, M. L., Tramo, M. J., Herron, D. M., Hermann, A., Loftus, W. C., Bazell, J., and Gazzaniga, M. S. 1989. Brainprints: Computer-generated two-dimensional maps of the human cerebral cortex *in vivo. J. Cogn. Neurosci.* **1:** 88–117.

Kraus, J. D. 1984. *Electromagnetics.* McGraw-Hill, Tokyo.

Landau, L. D., and Lifshitz, E. M. 1959. *Theory of Elasticity.* Pergamon Press, London.

Laroche, S. 1998. Managing very large-scale digital images in microscopy. *Eur. Microsc. Anat.* **7:** 25–27.

Levinthal, C., and Ware, R. 1972. Three-dimensional reconstruction from serial sections. *Nature* **236:** 207–210.

Lorenson, W. E., and Cline, H. E. 1987. Marching cubes: A high resolution 3D surface construction algorithm. *Comp. Graph.* **21:** 163–169.

Mountcastle, V. B. 1997. The columnar organization of the neocortex. *Brain* **120:** 701–722.

Merker, B. 1983. Silver staining of cell bodies by means of physical development. *J. Neurosci. Methods* **9:** 235–241.

Montgomery, K. 1996. *Automated Reconstruction of Neural Elements from Transmission Electron Microscope Images.* PhD Thesis, University of California, Santa Cruz.

Pakkenberg, B., and Gundersen, H. J. G. 1997. Neocortical neuron number in humans: Effect of sex and age. *J. Comp. Neurol.* **384:** 312–320.

Roland, P. E., and Zilles, K. 1998. Structural divisions and functional fields in the human cerebral cortex. *Brain Res. Rev.* **6:** 87–105.

Sarkissov, S. A., Filimonoff, I. N., Kononowa, E. P., Preobraschenskaja, I. S., and Kukuew, L. S. 1955. *Atlas of the Cytoarchitectonics of the Human Cerebral Cortex.* Medgiz, Moscow.

Sauer, B. 1983. Semi-automatic analysis of microscopic images of the human cerebral cortex using the grey level index. *J. Microsc.* **129:** 75–87.

Schleicher, A., Amunts, K., Geyer, S., Kowalski, T., Schormann, T., Palomero-Gallagher, N., and Zilles, K. 2000. A stereological approach to human cortical architecture: Identification and delineation of cortical areas. *J. Chem. Neuroanat.* **20:** 31–47.

Schleicher, A., Amunts, K., Geyer, S., Morosan, P., and Zilles, K. 1999. Observer-independent method for microstructural parcellation of cerebral cortex: A quantitative approach to cytoarchitectonics. *Neuroimage* **9:** 165–177.

Schleicher, A., Amunts, K., Geyer, S., Kowalski, T., and Zilles, K. 1998. Observer-independent cytoarchitectonic mapping of the human cortex using a stereological approach. *Acta. Stereol.* **17:** 75–82.

Schleicher, A., and Zilles, K. 1990. A quantitative approach to cytoarchitectonics: Analysis of structural inhomogeneities in nervous tissue using an image analyser. *J. Microsc.* **157:** 367–381.

Schleicher, A., Ritzdorf, H., and Zilles, K. 1987. Erster Ansatz zur objektiven Lokalisation von Arealgrenzen im Cortex cerebri. *Verh. Anat. Ges.* **81:** 867–868.

Schleicher, A., and Zilles, K. 1983. Der Einsatz automatischer Fernsehbildanalysatoren, Grenzen und Möglichkeiten. *Verh. Anat. Ges.* **77:** 189–199.

Schleicher, A., Zilles, K., and Kretschmann, H.-J. 1978. Automatische Registrierung und Auswertung eines Grauwertindex in histologischen Schnitten. *Verh. Anat. Ges.* **72:** 413–415.

Schmitt, O., and Eggers, R. 1997a. Systematic investigations of the contrast results of histochemical stainings of neurons and glial cells in the human brain by means of image analysis. *Micron* **28:** 197–215.

Schmitt, O., and Eggers, R. 1997b. High contrast and homogeneous staining of paraffin sections of whole human brains for three dimensional ultrahigh resolution image analysis. *Biotech. Histochem.* **73:** 44–51.

Schmitt, O., Almert, U., Mecke, E., and Eggers, R. 1998. Die quantitative Zytoarchitektonik der Areale nach Brodmann des menschlichen Cortex cerebri. *Focus MUL* **15:** 144–155.

Schmitt, O., and Eggers, R. 1999. Flat-bed scanning as a tool for quantitative neuroimaging. *J. Microsc.* **196:** 337–346.

Schmitt, O., Eggers, R., Modersitzki, J., Obelöer, W., and Lustig, G. 1999a. Multidimensional profiling of elastic deformed particle systems—A first approach. First Vogt-Brodmann Symposium. Perspectives of Architectonic Brain Mapping, Book of Abstracts p. 75.

Schmitt, O., Modersitzki, J., and Obelöer, W. 1999b. The human neuroscanning project. *NeuroImage* **9:** S22.

Schormann, T., and Zilles, K. 1998. Three-dimensional linear and nonlinear transformations: An integration of light microscopical and MRI data. *Hum. Brain. Mapp.* **6:** 339–347.

Schwartz, E. L., and Merker, B. 1986. Computer-aided neuroanatomy: Differential geometry of cortical surfaces and an optimal flattening algorithm. *IEEE Comp. Graph. Appl.* **6:** 36–44.

Schwarz, H. R. 1988. Numerische Mathematik. B. G. Teubner, Stuttgart.

Semendeferi, K., Armstrong, E., Schleicher, A., Zilles, K., and van Hoesen, G. W. 1998. Limbic frontal cortex in hominoids: A comparative study. *Am. J. Phys. Anthrop.* **106:** 129–155.

Smith, G. E. 1907. A new topographical survey of the human cerebral cortex, being an account to the distribution of the anatomically distinct cortical areas and their relationship to the cerebral sulci. *J. Anat.* **41:** 237–254.

Sokolnikoff, I. S. 1956. *Mathematical Theory of Elasticity.* McGraw-Hill, New York.

Van Essen, D. C., and Maunsell, J. H. R. 1980. Two-dimensional maps of the cerebral cortex. *J. Comp. Neurol.* **191:** 255–281.

von Economo, C., and Koskinas, G. N. 1925. *Die Cytoarchitektonik der Hirnrinde des erwachsenen Menschen.* Springer, Berlin.

West, M. J., Coleman, P. D., and Flood, D. G. 1988. Estimating the number of granule cells in the dentate gyrus with the disector. *Brain Res.* **448:** 167–172.

West, M. J., and Gundersen, H. J. G. 1990. Unbiased stereological estimation of the number of neurons in the human hippocampus. *J. Comp. Neurol.* **296:** 1–22.

West, M. J. 1990. Stereological studies of the hippocampus: A comparison of the hippocampal subdivisions of diverse species including hedgehogs, laboratory rodents, wild mice and men. *Prog. Brain. Res.* **83:** 13–36.

West, M. J., Slomianka, L., and Gundersen, H. J. G. 1991. Unbiased stereological estimation of the total number of neurons in the subdivisions of the rat hippocampus using the optical fractionator. *Anat. Rec.* **231:** 482–497.

West, M. J. 1993. Regionally specific loss of neurons in the aging human hippocampus. *Neurobiol. Aging* **14:** 287–293.

West, M. J., Coleman, P. D., Flood, D. G., and Troncoso, J. C. 1994. Differences in the pattern of hippocampal neuronal loss in normal ageing and Alzheimer's disease. *Lancet* **344:** 769–772.

West, M. J., and Slomianka, L. 1998. Total number of neurons in the layers of the human entorhinal cortex. *Hippocampus* **8:** 69–82.

Wree, A., Zilles, K., and Schleicher, A. 1981. A quantitative approach to cytoarchitectonics. VII. The areal pattern of the cortex of the Guinea pig. *Anat. Embryol.* **162:** 81–103.

Wree, A., Schleicher, A., and Zilles, K. 1982. Estimation of volume fractions in nervous tissue with an image analyzer. *J. Neurosci. Meth.* **6:** 29–43.

Wree, A., Zilles, K., and Schleicher, A. 1983. A quantitative approach to cytoarchitectonics. VIII. The areal pattern of the cortex of the albino mouse. *Anat. Embryol.* **166:** 333–353.

Xu, C., Pham, D. L., Rettmann, M. E., Yu, D. N., and Prince, J. L. 1999. Reconstruction of the human cerebral cortex from magnetic resonance images. *IEEE Trans. Med. Imag.* **18:** 467–480.

Zilles, K., Schlaug, G., Matelli, M., Luppino, G., Schleicher, A., Qu, M., Dabringhaus, A., Seitz, R., and Roland, P. E. 1995. Mapping of human and macaque sensorimotor areas by integrating architectonic, transmitter receptor, MRI and PET data. *J. Anat.* **187:** 515–537.

Zahn, M. 1979. *Electromagnetic Field Theory.* Wiley.